International Journal of Engineering Trends and Technology
ISSN: 2231 – 5381 /doi:10.14445/22315381/IJETT-V69I8P217
Volume 69 Issue 8, 138-144, August, 2021

Separability Analysis of The Band Combinations For Land Cover Classification of Satellite Images

Keerti Kulkarni[1,*], Dr. P. A. Vijaya[2]

[1]*Asst. Professor, Department of Electronics and Communication Engineering, BNM Institute of Technology, Bangalore, Karnataka, India.*
[2]*Professor and Head of Department, Department of Electronics and Communication Engineering, BNM Institute of Technology, Bangalore, Karnataka, India.*

keerti_p_kulkarni@yahoo.com

Abstract: *Land cover classification is one of the important applications of satellite images. The accuracy of the classification process depends on the feature selection. In multispectral satellite images, the separability of the features depends on the band combinations used. This work demonstrates the change in the accuracy of the classifiers with different band combinations and different distance measures used for analyzing the separability. Landsat-8 images have been classified into four land cover classes using the Maximum Likelihood (ML) Classifier, Minimum Distance (MD) Classifier, and the Spectral Angle (SA) mapper. The spectral separability between each of the land cover classes is analyzed for the band combinations of 3-2, 4-3-2, 3-2-1, 7-6-5-4, 7-6-5-4-3, using the Jeffries-Matusita Distance measure, the Euclidean Distance, and the spectral angle measure. It is shown that maximum separability and hence the optimal accuracy of 85.81% is obtained with a SA mapper using the spectral angle measure on a three-band combination of 4-3-2. An accuracy of 80.12% is achieved with an ML classifier using Jeffries-Matusita distance measure with a band combination of 4-3-2. Lastly, the MD classifier gives an accuracy of 76.56% using the Euclidean distance measure with a band combination of 4-3-2.*

Keywords: *Band combination, Euclidean Distance, Jeffries-Matusita Distance, Maximum Likelihood Classifier, Minimum Distance Classifier, Spectral angle, Spectral Angle Mapper.*

I. INTRODUCTION

Machine learning algorithms have often been used for the land cover classification of satellite images. The satellite images are either multispectral (3-10 bands) or hyperspectral (100s of bands). Each land cover class has a unique ***spectral signature***. The values of these spectral signatures are different in different bands, as each of the bands operates at a different wavelength. If the atmospheric effects are not taken into consideration, then the spectral signatures do not actually represent the values reflected from the surface of the earth. Hence the need for atmospheric correction. The spectral signatures of the different land cover types serve as the features for discriminating the various classes. For a learning algorithm to produce accurate results, the features have to be separable. This separability depends on how far apart the spectral signatures are placed in an N-dimensional space. Here, N denotes the number of bands under consideration. The spectral distance or the separability of the classes can be evaluated by a variety of distance measures, such as Euclidean distance, spectral angle, and the Jeffries-Matusita distance. It is important to measure the separability of the classes (by using the distance metric or the angle metric) in each of the band combinations before deciding which one is to be used. For the same classifier, keeping all the other parameters (number of training pixels) constant, a band combined with the greatest distance measure between the classes (greatest separability) will produce the highest classification accuracy. At the same time, different classifiers give different accuracies with different distance measures also. *This work hence analyses the separability of the spectral signatures in five different band combinations, using two distance metrics and an angle metric.*

II. LITERATURE SURVEY

Generally, a land cover classification problem deals with the semantic segmentation of the raw satellite images. The first step in this kind of semantic segmentation is the preparation of labeled training samples (Rogan et al., 2003, Elhag et al., 2013). These classes are labeled depending on their separability index (Friedl et al., 2010, Congalton & Green, 2008). This index is a discriminating factor, which is helpful in classifying the class of a pixel. Machine learning algorithms for this classification can be unsupervised when there is no spectral information available (Congalton & Green, 2008). When the spectral signature information is available, it can be exploited to discriminate between the classes (Kulkarni & Vijaya, 2019). Supervised classification also assumes that each of the spectral classes can be described by a probability distribution function (Richards & Richards, 1999, Gislason et al., 2006). Each of the bands of the LANDSAT potentially contributes to the information required for the land cover classification. But there will be redundancy in the information provided by each band if the bands themselves are highly correlated (Gong et al., 2013). Hence, only a small subset of all the bands available can be used. The identification of the subsets to be used can be categorized into two basic approaches. The analysis is

based either on calculating the eigenvalues (and eigenvectors) (Li et al., 2014) or separability analysis (Lunetta & Balogh, 1999). Separability analysis deals with calculating the statistical distance between the spectral classes. A variety of measures for calculating the distance are available in the literature (Davis et al., 1978, Mallinis et al., 2004). Each band has its own unique use for the identification of the land cover. For example, Band 1 can identify water, whereas band 7 can identify the urban areas. A near-infrared band can be used to identify the vegetation (ersi.com, Coggeshall & Hoffer, 1973). The performance of the classifier may actually degrade if the number of features (the number of bands) is increased (Duda et al., 1973). Separability analysis can also be carried out depending on the spectral indices like Normalized Difference Vegetation Index (NDVI) and other indices derived from the basic bands (Deng & Wu, 2012). The separability measures can be parametric or nonparametric (Huang et al., 2016). A transformed divergence method can also be used for the separability analysis (Dhaka et al., 2013). Rather than evaluating the spectral separability, the spectral similarity can be measured using the indices (Ye & Chul-Soo, 2020). S. Amelinckx, 2010 has summarized the separability analysis for the grasslands.

III. METHODOLOGY

The methodology adopted for the land cover classification is shown in Figure 1. The steps are briefly explained below.

A. Raw Satellite Images of the study area

The raw satellite images are the LANDSAT-8 images which have 11 bands. Band 1 to band-7 and band-9 have a resolution of 30 meters, band-8, which is a panchromatic band, has a resolution of 15 meters, and band-10 and band-11 have a resolution of 100 meters. All the bands encompass a different non-overlapping frequency spectrum.

The study area is the Bangalore Urban district. Bangalore is the capital city of the southern state of Karnataka in India. The area is majorly an urban area, where its landscape is predominantly heterogeneous. This geographical area is then classified according to the four land cover types, namely, water, vegetation, built-up, and soil.

LANDSAT-8 images dated 19th April 2021 have been downloaded. The actual tile of the satellite images has a larger geographical area. This is clipped to the required district boundaries by using a vector shapefile.

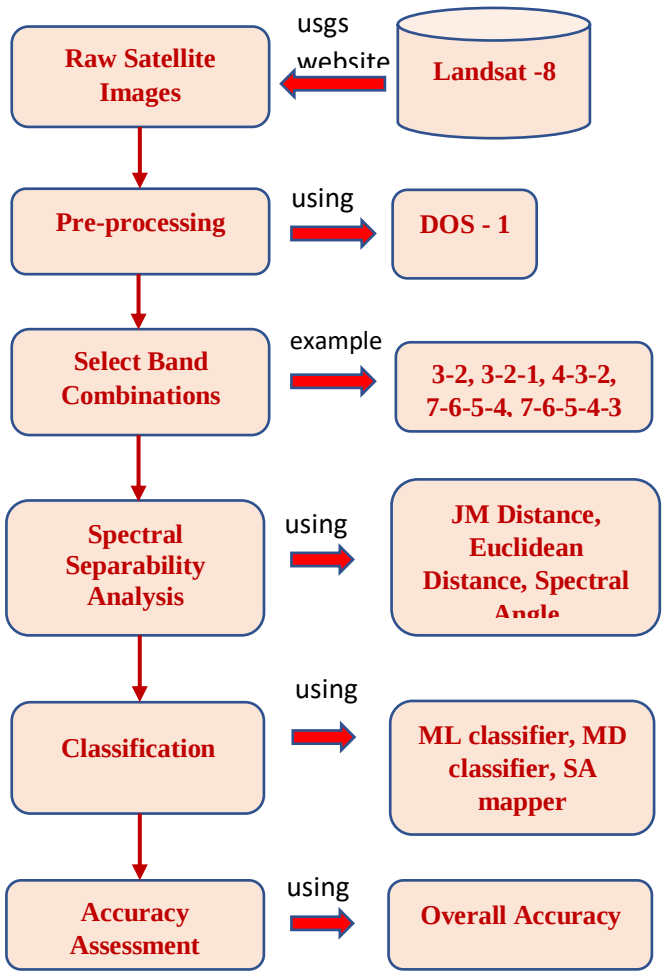

Figure 1: Methodology of the proposed research work

B. Pre-processing

The first step after downloading the required dataset is correcting the raw images for the atmospheric defects. This constitutes the pre-processing step. Dark Object Subtraction – 1 is a standard algorithm used for atmospheric correction. One more important reason for the atmospheric correction is that the separability between the classes is enhanced after the procedure, because of which histogram equalization need not be done.

C. Select Band Combinations

The band combinations indicate how the bands can be stacked one above the other to achieve a combined effect visually. Different spectral signatures manifest themselves differently in different bands. For example, a band combination of (4-3-2) is the true color composite, where the vegetation appears as green, water is black and urban areas appear white or grey. In contrast, there is also a false-color composite (3-2-1) where vegetation appears as red, water appears as black, and the built-up areas appear as purple or white. In this work, five different sets have been chosen, and their separability analyzed.

D. Spectral Separability Analysis

The spectral signature of the land cover class is unique and hence acts as the distinguishing factor for the classification. Different land cover classes have different

spectral signatures. For example, water reflects only up to 10% of the incident energy back to the sensor; hence it appears as a black form on the satellite image. Vegetation reflects 30% - 45% of the incident energy, soil reflects 20% - 30% of the incident energy and built-up areas reflect 10% - 20% of the incident energy back to the sensors. Even though this is a feature for the classification, the reflected energies and hence the spectral signatures are more pronounced in some bands as compared to some other bands. Hence the need for the spectral signature separability analysis for different band combinations in an N-dimensional space. Spectral Separability analysis is carried out by calculating the three distance/angle measures described in Section 5.

E. Distance Measures and Classifiers

The separability analysis is carried out using the distance measures as described below. Along with each distance measure, a supervised classifier that is best suited to that particular distance measure is also described.

a) Jeffries-Matusita (JM) Distance.

It is calculated between all the individual class probability distributions for different band combinations. JM distance calculates the separability between a pair of the probability distribution of the training classes. The formula for Jeffries-Matusita Distance is given by

$$JM_{ci,cj} = \sqrt{2(1 - e^{-B})} \quad [1]$$

Where B is the Bhattacharya distance given by

$$B = \frac{1}{8}(\mu_i - \mu_j)^T \left(\frac{C_i + C_j}{2}\right)^{-1} (\mu_i - \mu_j) + \frac{1}{2}\ln\left(\frac{\left|C_i + C_j/2\right|}{\sqrt{|C_i| + |C_j|}}\right) \quad [2]$$

Where

i **and** j = the two signature classes being compared

C_i = Covariance matrix of signature i

C_j = Covariance matrix of signature j

μ_i = mean of signature i

μ_j = mean of signature j

$|C_i|$ = determinant of C_i

The JM distance gives a minimum value of 0 when the signatures are similar and a maximum value of √2 when the signatures are very distinct. The main advantage of using the JM distance is that it tends to suppress the high separability values, and the low separability values are emphasized. This gives a fairly better idea of the separability compared to the Euclidean distance, where the minimum value is 0, but the maximum value is unbounded.

b) Maximum Likelihood Classifier.

It works on the principle of calculating the probability distribution of each pixel. If the probability that a pixel belongs to ***class-i*** is greater than the probability that the pixel belongs to ***class-j***, then it is classified as belonging to ***class-i***.

The discriminant function is calculated for every pixel as:

$$g_k(x) = \ln p(C_k) - \frac{1}{2}\ln|\sum k| - \frac{1}{2}(x - y_k)^t \sum_k^{-1}(x - y_k) \quad [3]$$

Where,

C_k = land cover class k;

x = spectral signature vector of an image pixel;

$p(C_k)$ = probability that the correct class is Ck;

$|\sum k|$ = determinant of the covariance matrix of the data in class Ck;

$\sum_k^{-1}(x - y_k)$ = inverse of the covariance matrix;

y_k = spectral signature vector of class k.

Therefore:

$$x \in C_k \leftrightarrow g_k(x) > g_j(x) \forall\, k \neq j \quad [4]$$

The discriminant function for the ML classifier is shown in Figure 2

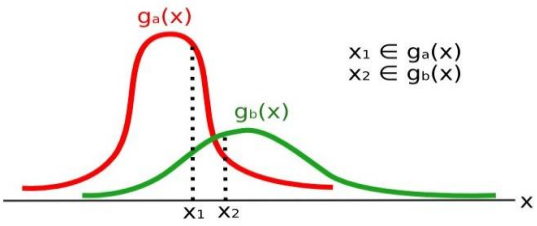

Figure 2: Discriminant Functions for an ML classifier

c) Euclidean distance.

Euclidean distance is calculated between the spectral signature vectors of pixels belonging to different classes. Mathematically,

$$d(x, y) = \sqrt{\sum_{i=1}^{n}(first\ spectral\ vector_i - second\ spectral\ vector_i)^2} \quad [5]$$

Where,

n = number of image bands under consideration.

The minimum value for the Euclidean distance is 0 (same class) and increases as the separability between the classes

increases. Since there is no upper bound on the Euclidean distance theoretically, here, the values are normalized to 1, using the z-score normalization. Therefore, a value of 1 indicates maximum separability between the classes.

d) Minimum Distance Classifier.

In the MD classifier, Euclidean distance is calculated for every pixel, and it is assigned a class for which the spectral signature has a minimum distance using the discriminant function

$$\boldsymbol{x} \in \boldsymbol{C_k} \leftrightarrow \boldsymbol{ED}(\boldsymbol{x}, \boldsymbol{y_k}) \leq \mathbf{ED}(\boldsymbol{x}, \boldsymbol{y_j}) \forall\, \boldsymbol{k} \neq \boldsymbol{j} \quad [6]$$

5.5 Spectral Angle

It calculates the angle between the spectral signatures of the training pixels and the image pixels by using equation 7 given below. The summation is carried out for all 4 classes.

$$\boldsymbol{SA}(\boldsymbol{x}, \boldsymbol{y}) = \boldsymbol{cos}^{-1}\left(\frac{\sum_{i=1}^{n}(\boldsymbol{spectral\ vector\ of\ im}) * (\boldsymbol{spectral\ vector\ of\ training})}{(\sum(\boldsymbol{spectral\ vector\ of\ im})^2)^{1/2} * (\sum(\boldsymbol{spectral\ vector\ of\ training})^2}\right) \quad [7]$$

Where,

n = number of image bands under consideration.

The separability can be visualized as given in Figure 3

5.6 Spectral Angle Mapper.

Hence the pixel is classified as belonging to the class having the least angle. Mathematically,

$$\boldsymbol{x} \in \boldsymbol{C_k} \leftrightarrow \boldsymbol{SA}(\boldsymbol{x}, \boldsymbol{y_k}) \leq \mathbf{SA}(\boldsymbol{x}, \boldsymbol{y_j}) \forall\, \boldsymbol{k} \neq \boldsymbol{j} \quad [8]$$

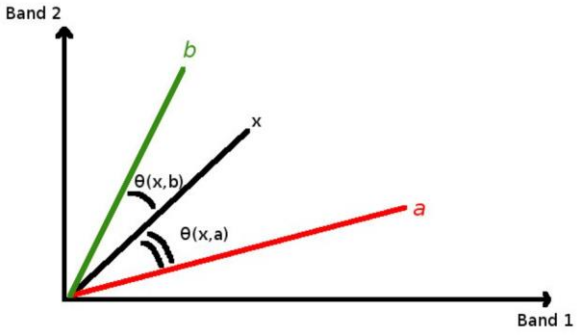

Figure 3: Separability measure using spectral angle.

The minimum value for the spectral angle is 0° (same class), and the maximum is 90° (maximum separability).

In this work, the ML classifier uses the JM distance as a separability measure, MD uses the Euclidean distance, and the SA mapper uses the spectral angle measure for separability.

VI. Classification Accuracy

Finally, the classification accuracy of the classifier for all the five band combinations is calculated. Classification accuracy is defined as the ratio of the total number of pixels correctly classified to the total number of pixels.

VII. RESULTS

Figure 4 and Figure 5 show the spectral signatures before and after the atmospheric correction. It is easier to visually note the separability in the second case. Also, Figure 5 shows the spectral signatures plot for a band combination of 4-3-2. Similar spectral signature plots are obtained for the other band combinations.

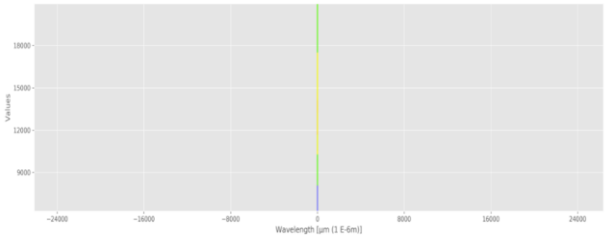

Figure 4: Spectral Signatures before the Atmospheric Correction

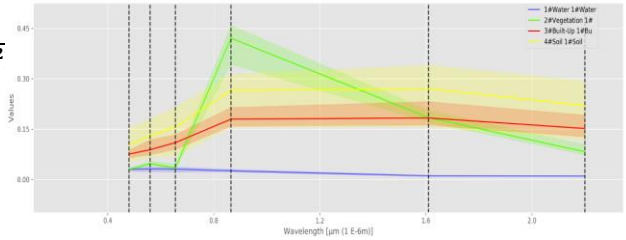

Figure 5: Spectral Signatures after the Atmospheric Correction

Table 1 shows the Jeffries-Matusita distance or the separability matrix between the classes for a two-band combination of 3-2. Table 2 and Table 3 show the separability matrix for a three-band combination of 3-2-1 and 4-3-2, respectively. Table 4 shows the separability matrix for a four-band combination of 7-6-5-4, and Table 5 shows the separability matrix for a five-band combination of 7-6-5-4-3. Similarly, the separability analysis is done for the same set of band combinations using Euclidean distance and Spectral angle.

Table 1: Separability Matrix for a 2-band combination (3-2)

		Water	Vegetation	Built-Up	Soil
JMD	Water	0.1	0.83	1.01	0.97
	Vegetation	0.83	0.1	0.93	0.75
	Built-Up	1.01	0.93	0.1	0.81
	Soil	0.97	0.75	0.81	0.1
ED	Water	0.05	0.7	0.72	0.73
	Vegetation	0.7	0.06	0.76	0.7
	Built-Up	0.72	0.76	0.09	0.73
	Soil	0.73	0.7	0.73	0.09
SA	Water	2	70	72	75
	Vegetation	70	3	74	69
	Built-Up	72	74	3	71
	Soil	75	69	71	2

Table 2: Separability Matrix for a 3-band combination (3-2-1)

		Water	Vegetation	Built-Up	Soil
JMD	Water	0.02	1.1	1.19	1.05
	Vegetation	1.1	0.1	1.2	0.96
	Built-Up	1.19	1.2	0	0.91
	Soil	1.05	0.96	0.91	0.02
ED	Water	0.03	0.75	0.8	0.81
	Vegetation	0.75	0.02	0.82	0.79
	Built-Up	0.8	0.82	0.01	0.82
	Soil	0.81	0.79	0.82	0.02
SA	Water	1	72	74	75
	Vegetation	72	2	76	71
	Built-Up	74	76	1	72
	Soil	75	71	72	1

Table 3: Separability Matrix for a 3-band combination 4-3-2

		Water	Vegetation	Built-Up	Soil
JMD	Water	0.01	1.2	1.29	1.01
	Vegetation	1.2	0.1	1.26	0.91
	Built-Up	1.29	1.26	0	1.11
	Soil	1.01	0.91	1.11	0.01
ED	Water	0.01	0.82	0.85	0.81
	Vegetation	0.82	0.01	0.85	0.81
	Built-Up	0.85	0.85	0.01	0.86
	Soil	0.81	0.81	0.86	0.01
SA	Water	1	80	82	85
	Vegetation	80	1	84	79
	Built-Up	82	84	1	83
	Soil	85	79	83	1

Table 4: Separability Matrix for a 4-band combination 7-6-5-4

		Water	Vegetation	Built-Up	Soil
JMD	Water	0.02	1.1	1.19	1.05
	Vegetation	1.1	0.1	1.2	0.96
	Built-Up	1.19	1.2	0	0.91
	Soil	1.05	0.96	0.91	0.02
ED	Water	0.02	0.79	0.78	0.76
	Vegetation	0.79	0.01	0.76	0.71
	Built-Up	0.78	0.76	0.01	0.79
	Soil	0.76	0.71	0.79	0.03
SA	Water	2	71	72	74
	Vegetation	71	2	72	73
	Built-Up	72	72	1	74
	Soil	74	73	74	1

Table 5: Separability Matrix for a 5-band combination 7-6-5-4-3

		Water	Vegetation	Built-Up	Soil
JMD	Water	0.01	1.1	1.12	0.92
	Vegetation	1.1	0	0.96	0.73
	Built-Up	1.12	0.96	0.01	0.75
	Soil	0.92	0.73	0.75	0.1
ED	Water	0.03	0.78	0.72	0.76
	Vegetation	0.78	0.02	0.73	0.76
	Built-Up	0.72	0.73	0.03	0.75
	Soil	0.76	0.76	0.75	0.03
SA	Water	3	73	71	76
	Vegetation	73	3	71	76
	Built-Up	71	71	2	79
	Soil	76	76	79	1

The average separability using the three distance measures on different band combinations is summarized in Table 6.

Table 6: Average separability between the classes for the different band combinations

Distance Measure → / Band Combinations ↓	Jeffries Matusita	Euclidean Distance	Spectral Angle
3-2	0.6875	0.72	71.8
3-2-1	0.81	0.8	73.3
4-3-2	0.855	0.83	82.16
7-6-5-4	0.81	0.76	72.66
7-6-5-4-3	0.705	0.75	74.33

From the above table, it is found that the maximum average separability is achieved with a band combination of 4-3-2 for all the distance measures. Hence the next step is to map the land cover using three classifiers, namely, ML classifier, MD classifier, and SA mapper. These three classifiers use JM distance, Euclidean distance, and spectral angle measures, respectively. The map is classified using the band combination of 4-3-2. The results are summarized in Table 7. It is important to note here that the ML classifier uses the JM distance, the MD classifier uses the Euclidean distance, and the SA mapper uses the spectral angle measure. Figure 6a shows the land cover map obtained using an ML classifier using the band combination of 4-3-2. Figure 6b shows the land cover map obtained using an MD classifier using the band combination of 4-3-2. Figure 6c shows the land cover map obtained using an SA mapper using the band combination of 4-3-2.

Table 7: Classification Accuracy of the three classifiers using the three distance measures

Distance Measure → / Classifiers ↓	Jeffries Matusita	Euclidean Distance	Spectral Angle
ML	80.12		
MD		76.56	
SA			85.81

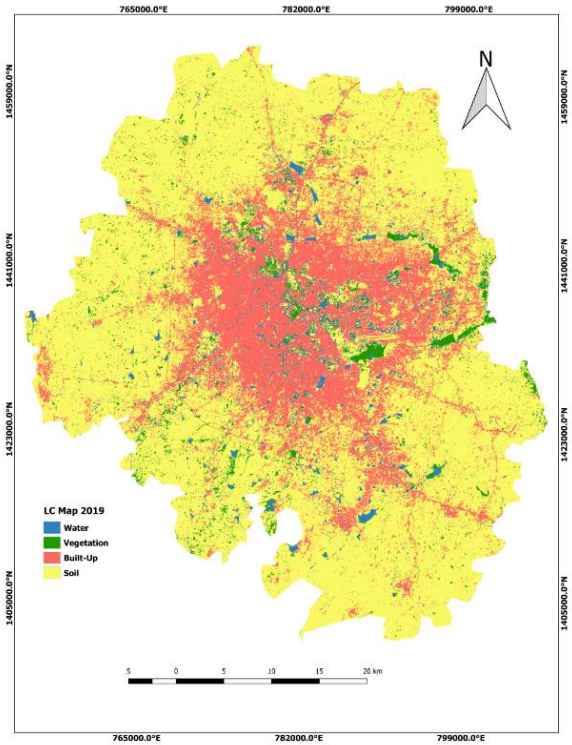

Figure 6a: land cover map using the ML classifier using JM distance with a 4-3-2 band combination.

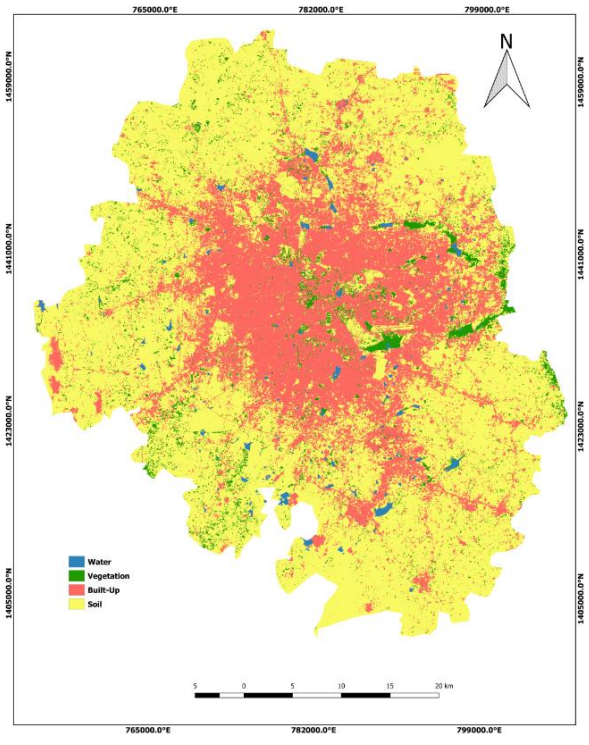

Figure 6b: land cover map using the MD classifier using Euclidean distance with a 4-3-2 band combination.

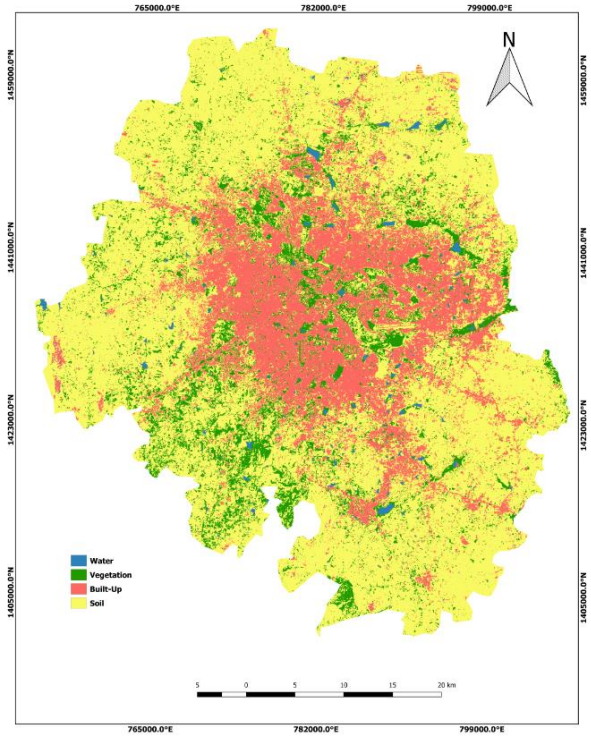

Figure 6c: land cover map using the SA mapper using spectral angle with a 4-3-2 band combination.

VIII. DISCUSSION

The main aim of this work was to analyze the separability of the spectral signatures in different band combinations. To achieve this, five different band combinations were used and were analyzed using three different separability measures. The separability tables show that a maximum separability between the spectral signatures is obtained with a band combination of 4-3-2. This result holds true for the other separability measures also. This is logical also because the bands 4, 3, and 2 represent the RGB or the visual bands. Hence the visual interpretation of the separability of the signatures is better in this band combination. Even if the number of bands increases, the separability of the signatures (and hence the accuracy of the classifiers) does not improve. This result also upholds the curse of dimensionality (Bellman, 1953), which says that the increase in the number of features does not always increase the accuracy of the classifier. Hence, using the band combination of 4-3-2, the accuracy obtained from a SA mapper is 85.71%, the accuracy of the MD classifier is 76.56%, and the accuracy of the ML classifier is 80.12%.

IX. CONCLUSION AND FUTURE WORK

This work has tried to implement the various distance and angle-based separability measures for different band combinations. This analysis provides a basis on which a classifier model can be built to provide better classification accuracy. Choosing the band combination which provides better separability results in optimal performance of the classifiers, as shown in this work.

All the three classifiers explored here are parametric classifiers, which extract the information for calculating the covariance matrix from the training data itself. Once the parameters are set, then no amount of increase in the training data is going to increase the classification accuracy. The improvement in the accuracy can be further explored by using a different distance measure. Also, non-parametric approaches to the classification process, where hyperparameters can be tuned, can be used to further improve the classification accuracy.

ACKNOWLEDGEMENTS

The authors sincerely thank the management of the BNM Institute of Technology for providing the necessary infrastructure to carry out the project work. The authors are also indebted to the Visveswaraya Technological University for providing a suitable platform to carry out the research work.

REFERENCES

[1] C. Deng and C. Wu., BCI: A biophysical composition index for remote sensing of urban environments, Remote Sens. Environ., 127 (2020) 247–259.

[2] Congalton, R.G., and K. Green., Assessing the accuracy of remotely sensed data: principles and practices, CRC press, (2008).

[3] Coggeshall, M.E. and R.M. Hoffer., Basic forest cover mapping using digitized remote sensor data and automated data processing techniques, LARS Technical Reports. Paper 23. (1973). http://docs.lib.purdue.edu/larstech/23

[4] Davis, S.M., et al., Remote sensing: the quantitative approach". New York, McGraw-Hill International Book Co, L (1978).

[5] Duda, R.O., P.E. Hart, and D.G. Stork ., Pattern classification, Wiley New York, 2 (1973).

[6] Elhag, M., A. Psilovikos, and M. Sakellariou., Detection of land cover changes for water recourses management using remote sensing data over the Nile Delta Region, Environment, Development and Sustainability, 15(5) (2013)1189-1204.

[7] Friedl, M.A., et al., MODIS Collection 5 global land cover: Algorithm refinements and characterization of new datasets. Remote sensing of Environment, 114(1) (2010) 168-182.

[8] Gislason, P.O., J.A. Benediktsson, and J.R. Sveinsson., "Random forests for land cover classification. Pattern Recognition Letters, 27(4) (2006) 294-300.

[9] Gong, P., et al., Finer resolution observation and monitoring of global land cover: First mapping results with Landsat TM and ETM+ data. International Journal of Remote Sensing, 34(7) (2013) 2607-2654.

[10] H. Huang et al., Separability Analysis of Sentinel-2A Multi-Spectral Instrument (MSI) Data for Burned Area Discrimination, Remote Sensing 8(10) (2016) 873 https://doi.org/10.3390/rs8100873

[11] Li, C., et al., Comparison of classification algorithms and training sample sizes in urban land classification with Landsat thematic mapper imagery. Remote Sensing, 6(2) (2014) 964-983

[12] Lunetta, R.S. and M.E. Balogh., Application of multi-temporal Landsat 5 TM imagery for wetland identification. Photogrammetric Engineering and Remote Sensing. 65(11) (1999) 1303-1310.

[13] Mallinis, G. et al., Forest parameters estimation in a European Mediterranean landscape using remotely sensed data. Forest Science, 50(4) (2004) 450-460.

[14] Kulkarni K, Dr. P. A. Vijaya., Parametric Approaches to Multispectral Image Classification using Normalized Difference Vegetation Index, International Journal of Innovative Technology and Exploring Engineering, 9(2S) (2019) DOI: 10.35940/ijitee.B1061.1292S19, pp 611-615.

[15] Kulkarni K, Dr. P. A. Vijaya ., Experiment of Multispectral Images using Spectral Angle Mapper Algorithm for Land Cover Classification, International Journal of Innovative Technology and Exploring Engineering, 8(6S4),(2019) 96-99.

[16] Richards, J.A. and J. Richards ., Remote sensing digital image analysis, 3 (1999), Springer.

[17] Rogan, J., et al., Land-cover change monitoring with classification trees using Landsat TM and ancillary data, Photogrammetric Engineering & Remote Sensing, 69(7) (2003) 793-804.

[18] S. Amelinckx ., Spatial and spectral separability of grasslands in the inner Turku Archipelago using landsat thematic mapper satellite imagery., Masters Thesis, University of Turku, Finland, (2010).

[19] Dhaka Suman, Shankar Hari, P.S.Roy, Kiran Raj ., IRS P6 LISS-IV Image Classification using Simple, Fuzzy Logic and Artificial Neural Network Techniques: A Comparison Study, International Journal of Technical Research & Science, 1(2) (2016).

[20] Ye, Chul-Soo, Evaluating the Contribution of Spectral Features to Image Classification Using Class Separability, Korean Journal of Remote Sensing, 36(1) (2020) 55-65, https://doi.org/10.7780/kjrs.2020.36.1.5

[21] Bellman, R ., Dynamic programming, Princeton University Press, (1953).

[22] https://www.esri.com/arcgis-blog/products/product/imagery/band-combinations-for-landsat-8/

[23] Mishra P.K, A. Rai, and S. C. Rai, Land use and land cover change detection using geospatial techniques in the Sikkim Himalaya, India, Egypt. J. Remote Sens. Sp. Sci., 23(2) (2020) 133–143.

[24] E. Venkateswarlu, T. Sivannarayana, and K. V. R. Kumar, A comparative analysis of Resources at-2 LISS-3 and LANDSAT-8 OLI imagery, Int. Arch. Photogramm. Remote Sens. Spat. Inf. Sci. - ISPRS Arch., 40(8) (2014) 987–989.

[25] Gandhi G. M., S. Parthiban, N. Thummalu, and A. Christy, Ndvi: Vegetation Change Detection Using Remote Sensing And Gis - A Case Study of Vellore District, Procedia Comput. Sci., 57 (2015) 1199–1210.